White Matter Changes in Comatose Survivors of Anoxic Ischemic Encephalopathy and Traumatic Brain Injury: Comparative Diffusion-Tensor Imaging Study[1]

Anke W. van der Eerden, MD
Omid Khalilzadeh, MD, MPH
Vincent Perlbarg, PhD
Julien Dinkel, MD, PhD
Paola Sanchez, MD
Pieter E. Vos, MD, PhD
Charles-Edouard Luyt, MD, PhD
Robert D. Stevens, MD, PhD
Nicolas Menjot de Champfleur, MD, PhD
Christine Delmaire, MD
Eleonore Tollard, MD
Rajiv Gupta, MD, PhD
Didier Dormont, MD, PhD
Steven Laureys, MD, PhD
Habib Benali, MD, PhD
Audrey Vanhaudenhuyse, PhD
Damien Galanaud, MD, PhD
Louis Puybasset, MD, PhD
For the NICER (Neuro Imaging for Coma Emergence and Recovery) Consortium

Purpose: To analyze white matter pathologic abnormalities by using diffusion-tensor (DT) imaging in a multicenter prospective cohort of comatose patients following cardiac arrest or traumatic brain injury (TBI).

Materials and Methods: Institutional review board approval and informed consent from proxies and control subjects were obtained. DT imaging was performed 5–57 days after insult in 49 cardiac arrest and 40 TBI patients. To control for DT imaging–processing variability, patients' values were normalized to those of 111 control subjects. Automated segmentation software calculated normalized axial diffusivity ($\lambda_{\parallel}$) and radial diffusivity ($\lambda_{\perp}$) in 19 predefined white matter regions of interest (ROIs). DT imaging variables were compared by using general linear modeling, and side-to-side Pearson correlation coefficients were calculated. *P* values were corrected for multiple testing (Bonferroni).

Results: In central white matter, $\lambda_{\parallel}$ differed from that in control subjects in six of seven TBI ROIs and five of seven cardiac arrest ROIs (all $P < .01$). The $\lambda_{\perp}$ differed from that in control subjects in all ROIs in both patient groups ($P < .01$). In hemispheres, $\lambda_{\parallel}$ was decreased compared with that in control subjects in three of 12 TBI ROIs ($P < .05$) and nine of 12 cardiac arrest ROIs ($P < .01$). The $\lambda_{\perp}$ was increased in all TBI ROIs ($P < .01$) and in seven of 12 cardiac arrest ROIs ($P < .05$). Cerebral hemisphere $\lambda_{\parallel}$ was lower in cardiac arrest than in TBI in six of 12 ROIs ($P < .01$), while $\lambda_{\perp}$ was higher in TBI than in cardiac arrest in eight of 12 ROIs ($P < .01$). Diffusivity values were symmetrically distributed in cardiac arrest ($P < .001$ for side-to-side correlation) but not in TBI patients.

Conclusion: DT imaging findings are consistent with the known predominance of cerebral hemisphere axonal injury in cardiac arrest and chiefly central myelin injury in TBI. This consistency supports the validity of DT imaging for differentiating axon and myelin damage in vivo in humans.

Online supplemental material is available for this article.

[1] From the Department of Neuroradiology (A.W.v.d.E., D.D., D.G.), the Neurosurgical ICU (P.S., L.P.), and the Medical ICU (C.E.L.), Hôpital Pitié-Salpêtrière, Assistance Publique–Hôpitaux de Paris, 47-83 boulevard de l'Hôpital, 75651 Paris Cedex 13, France; Departments of Radiology (A.W.v.d.E.) and Neurology (P.E.V.), Radboud University Nijmegen Medical Centre, Nijmegen, the Netherlands; INSERM, UMRS 678, Université Pierre et Marie Curie-Paris 6, Paris, France (V.P., H.B.); Department of Radiology, Massachusetts General Hospital, Boston, Mass (O.K., J.D., R.G.); Division of Neuroscience Critical Care, Department of Anesthesiology Critical Care Medicine, Johns Hopkins University School of Medicine, Baltimore, Md (R.D.S.); Department of Neuroradiology, Guy de Chauliac Hospital, Montpellier, France (N.M.d.C.); Department of Neuroradiology, Roger Salengro Hospital, Lille, France (C.D.); Department of Neuroradiology, Centre Hospitalier Universitaire, Rouen, France (E.T.); and Cyclotron Research Center, University of Liège, Liège, Belgium (S.L., A.V.). Received December 18, 2012; revision requested February 20, 2013; final revision received May 20; accepted May 29; final version accepted August 12. Supported by a grant from the French Ministry of Health (Projet Hospitalier de Recherche Clinique registration P051061 [2005]), Paris, France, and from the Agence Nationale de la Recherche, Paris France, for the program "investissements d'avenir" under agreement ANR-10-IAIHU-06 for the Paris Institute of Translational Neurosciences-IHU-A-ICM. **Address correspondence to** D.G. (e-mail: *galanaud@gmail.com*).

Cardiac arrest and traumatic brain injury (TBI) may lead to similar clinical presentations that include prolonged impaired consciousness, even though these two types of insult have vastly different pathophysiologic mechanisms. These differences are reflected in the spatial distribution of abnormalities over the brain. In TBI, shearing and acceleration-deceleration forces lead to diffuse axonal injury mostly in the central structures such as the brainstem and corpus callosum, often associated with contusions in the cerebral hemispheres (1). In cardiac arrest, the areas most vulnerable to damage are the watershed areas of the cerebral hemispheres (2–4).

Diffusion-tensor (DT) imaging provides information not only on lesion localization but also on the nature of white matter damage. The DT imaging parameter axial diffusivity (λ_1) depends chiefly on the diffusibility of water molecules parallel to a tract, whereas radial diffusivity ($\lambda_\perp$) assesses water diffusion perpendicular to the tract (5). Thus, changes in λ_1 are thought to be associated primarily with axonal damage, while changes in $\lambda\perp$ are thought to relate to myelin injury (6–8). These parameters provide greater anatomic and functional information than scalar DT imaging parameters such as fractional anisotropy and the apparent diffusion coefficient (6,9–13), which have been more extensively evaluated than λ_1 and $\lambda_\perp$. These constructs have been validated in animal models (6–8,14,15). Their meaning in humans has been less studied.

We hypothesized that the different pathophysiologic events occurring in the subacute phase after cardiac arrest and TBI have different effects on λ_1 and $\lambda_\perp$. The purpose of this study was to analyze the anatomic distribution of white matter pathologic abnormalities by using DT imaging in a multicenter prospective cohort of patients with impaired consciousness following cardiac arrest or TBI.

Advances in Knowledge

- In cardiac arrest, the predominant finding at diffusion-tensor (DT) imaging is a marked decrease in axial diffusivity (λ_1) (−8.9% in central regions, −9.1% in cerebral hemispheres), whereas in traumatic brain injury (TBI), the predominant finding is a marked increase in radial diffusivity ($\lambda_\perp$) (37.5% in central regions, 24.9% in cerebral hemispheres).
- The central brain structures show lower λ_1 and higher $\lambda_\perp$ values in TBI than in cardiac arrest (cardiac arrest vs TBI, $P < .01$ for λ_1 in the lower brainstem region and for $\lambda_\perp$ in the cerebral peduncles region and corpus callosum region); in the cerebral hemispheres regions, λ_1 and $\lambda_\perp$ are highly abnormal in both cardiac arrest and TBI, with the lowest λ_1 values occurring in cardiac arrest (cardiac arrest vs TBI, −9.1% vs −0.1%; $P < .01$) and the highest $\lambda_\perp$ values in TBI (TBI vs cardiac arrest, 24.9% vs 9.7%; $P < .01$).
- The known predominance of left-sided damage in TBI patients with poor clinical outcomes is attributable to left-sided predominance of $\lambda_\perp$ abnormalities and, to a lesser extent, λ_1 abnormalities ($P > .05$ for side-to-side correlations in five of six ROIs for $\lambda_\perp$ and in three of six ROIs for λ_1); this finding suggests greater asymmetry of edema and/or myelin damage than of axonal damage in TBI.

Implications for Patient Care

- Our findings help physicians understand the mechanisms underlying chronic consciousness impairments after TBI and cardiac arrest.
- Our findings encourage physicians who interpret DT imaging studies to take into account not only scalar variables such as fractional anisotropy and apparent diffusion coefficient but also vector variables such as λ_1 and $\lambda_\perp$.

Materials and Methods

The institutional review boards of the participating institutions approved this prospective study. All patients' next of kin and healthy control subjects gave informed consent. The patients and healthy control subjects were recruited during a study on the relevance of DT imaging biomarkers in the prediction of recovery of consciousness in patients after cardiac arrest and after TBI. In that study, the researchers used the same inclusion and exclusion criteria, the same clinical data and the same methods of magnetic resonance (MR) imaging acquisition and MR imaging analysis as were used in the present study. The study on the relevance of DT imaging biomarkers in the prediction of recovery of consciousness led to two articles, one for cardiac arrest (16) and the other for TBI (17), and the design is reported in more detail in those two previous articles (16,17). Two authors (V.P., a computer scientist with 10 years of experience, and D.G., a

Published online before print
10.1148/radiol.13122720 **Content codes:** MR NR

Radiology 2014; 270:506–516

Abbreviations:
DT = diffusion tensor
λ_1 = axial diffusivity
$\lambda_\perp$ = radial diffusivity
TBI = traumatic brain injury

Author contributions:
Guarantors of integrity of entire study, A.W.v.d.E., V.P., H.B., L.P.; study concepts/study design or data acquisition or data analysis/interpretation, all authors; manuscript drafting or manuscript revision for important intellectual content, all authors; approval of final version of submitted manuscript, all authors; literature research, A.W.v.d.E., O.K., P.S., P.E.V., R.D.S., E.T., R.G., L.P.; clinical studies, A.W.v.d.E., V.P., P.S., C.E.L., R.D.S., C.D., E.T., D.D., S.L., H.B., A.V., D.G., L.P.; experimental studies, P.S., R.D.S., S.L., D.G.; statistical analysis, A.W.v.d.E., O.K., V.P., J.D., P.S., R.D.S., R.G., H.B., L.P.; and manuscript editing, A.W.v.d.E., O.K., V.P., J.D., P.S., P.E.V., C.E.L., R.D.S., N.M.d.C., C.D., R.G., A.V., D.G., L.P.

Conflicts of interest are listed at the end of this article.

neuroradiologist with 15 years of experience) processed the DT imaging acquisitions. They had no access to the clinical information and outcome of the patients.

Patients

Consecutive patients were enrolled prospectively in eight intensive care units in Paris, Lille, Lyon, Montpellier, Nancy, Rouen, and Bordeaux in France and in Liège in Belgium following cardiac arrest or TBI between October 2006 and February 2010. Patients were eligible if they *(a)* were between 18 and 85 years old, and *(b)* had severe brain damage, as expressed by *(i)* inability to follow simple commands 7–28 days after the incident, unexplained by sedation, and *(ii)* a Glasgow Outcome Scale (18) score of 1 or 2 at 12 months after the injury or a Glasgow Outcome Scale score of 3 that was explained by cognitive and not purely physical impairment. On the basis of these inclusion criteria, 57 patients with cardiac arrest and 55 patients with TBI were eligible. Patients were excluded if they *(a)* had a central neurologic disease prior to cardiac arrest or TBI (n = 2); *(b)* had a penetrating head injury (n = 1); *(c)* were moribund (expected survival of < 24 hours) (n = 0); *(d)* had a contraindication to MR imaging (*n* = 4); or *(e)* were too unstable to be transported and to undergo MR imaging (*n* = 0). On the basis of their eligibility, we enrolled 54 patients with cardiac arrest and 51 patients with TBI. Of these, the MR imaging data in five patients with cardiac arrest and in 11 patients with TBI could not be evaluated because of a suboptimal MR imaging acquisition, as a result of motion (four cardiac arrest patients, five TBI patients), other artifacts (zero cardiac arrest patients, one TBI patient), or deviation in the MR imaging protocol (one cardiac arrest patient, one TBI patient), or because an insufficient number of healthy control subjects were imaged (zero cardiac arrest patients, four TBI patients). Finally, we included 49 of 57 patients with cardiac arrest (86%) and 40 of 55 patients with TBI (73%) with sufficient quality normalized DT imaging data. Demographic and clinical characteristics of the patients are summarized in Table 1.

Table 1

Demographics and Clinical Characteristics of the Patients

Variable	TBI Patients (*n* =40)	Cardiac Arrest Patients (*n* = 49)
Sex*		
Male	32 (80)	32 (65)
Female	8 (20)	17 (35)
Age (y)†	36 (19–76)	54 (19–85)
Male	36 (19–75)	55 (19–85)
Female	37 (19–76)	47 (20–77)
Site of patient recruitment‡		
Paris, France	9 (23)	44 (90)
Liège, Belgium	2 (5)	4 (8)
Lyon, France	3 (8)	0
Montpellier, France	7 (18)	0
Nancy, France	7 (18)	0
Rouen, France	5 (13)	0
Bordeaux, France	7 (18)	1 (2)
At arrival of the emergency team		
GCS score§	4 (3–7)	3 (3–15)
Hypotension‖	2 (5)	17 (35)
Hypoxemia#	14 (35)	19 (39)
At hospital admission		
Pupillary reflex absent on one or both sides**	13 (33)	6 (12)
Time from insult to MR imaging (d)†	22 (7–57)	11 (5–47)
GOS 12 mo after injury‡		
Score 1	21 (53)	42 (86)
Score 2	5 (13)	5 (10)
Score 3	14 (35)	2 (4)

Note.—GCS = Glasgow Coma Scale, GOS = Glasgow Outcome Scale. The site of patient recruitment at Lille, France, was a recruiting center, but all of the patients there had a favorable clinical outcome (GOS > 3 or GOS of 3 explained by physical impairment only). Therefore, none of the patients at that center were included in our analyses.

* Data are numbers of patients, and numbers in parentheses are percentages.

† Data are medians, and numbers in parentheses are ranges. $P < .001$ for differences between TBI patients and cardiac arrest patients.

‡ Data are numbers of patients, and numbers in parentheses are percentages. $P < .001$ for differences between TBI patients and cardiac arrest patients.

§ Data are medians, and numbers in parentheses are ranges.

‖ Hypotension was defined as systolic blood pressure less than 90 mm Hg. Data are numbers of patients, and numbers in parentheses are percentages. $P < .01$ for differences between TBI patients and cardiac arrest patients.

Hypoxemia was defined as oxygen saturation of blood of less than 90%. Data are numbers of patients, and numbers in parentheses are percentages.

** Data are numbers of patients, and numbers in parentheses are percentages. $P < .05$ for differences between TBI patients and cardiac arrest patients.

Cardiac Arrest

The cause of the cardiac arrest was primarily cardiac (cardiac arrest originating in the heart [eg, myocardial infarction]) in 39 of 49 patients (80%) and secondarily cardiac (cardiac arrest resulting from disease outside the heart [eg, severe hypoxia or hyperkalemia]) in 10 of 49 patients (20%). The mean duration of no flow before cardiopulmonary resuscitation was 5 minutes (interquartile range, 0–10 minutes). It took a median of 20 minutes (interquartile range, 10–36 minutes) for the circulation to become fully effective under cardiopulmonary resuscitation.

Hypothermia was induced in 29 of 49 patients (59%). At admission, the mean serum troponin I level was 0.48 ng/mL (0.48 μg/L), with an interquartile range of 0.1–4.4 ng/mL (0.1–4.4 μg/L).

Traumatic Brain Injury

TBI was caused by a motor vehicle accident in 26 of 40 cases (65%) (20 drivers or passengers [50%] and six pedestrians [15%]), by a fall in nine of 40 cases (23%), and by another mechanism in five of 40 cases (13%). On a computed tomography (CT) scan obtained within 48 hours of the TBI, six of 40 TBI patients (15%) had an epidural hematoma, 14 of 40 patients (35%) had a subdural hematoma, 34 of 40 patients (85%) had a subarachnoid hemorrhage, 27 of 40 patients (68%) had one or more contusions, and nine of 40 patients (23%) had a midline shift larger than 6 mm. None of the TBI patients had signs of ischemia on this early CT scan. Of 40 patients, 18 (45%) had a Marshall classification diffuse injury I–II, five (13%) had a Marshall classification diffuse injury III, one (3%) had a Marshall classification diffuse injury IV, and 15 (38%) had a mass lesion (eight patients had an evacuated mass lesion and seven patients had a nonevacuated mass lesion) (19). Fourteen of 40 TBI patients (35%) underwent a neurosurgical intervention.

Healthy Control Subjects

To control for multisite variability in DT imaging data, in each center we compared the patients' DT imaging values with those of a total of 111 healthy volunteers, with four to 51 control subjects per center; 60 of 111 (54%) were men and 51 (46%) were women (mean age, 33 years ± 3 [standard deviation]). These control subjects underwent MR imaging with the same acquisition parameters as the patients. Volunteers were recruited by the local principal investigator among staff members of each center. They gave written informed consent to study participation. Individuals with no history of neurologic disease requiring medical attention were eligible. We excluded volunteers with abnormalities in the morphologic sequences, as occurred in two individuals (two of 113, 2%): one with mild atrophy and another with asymptomatic white matter disease.

Clinical Data Collection

Data were prospectively collected by using standardized case report forms and a Web-based, encrypted, and centrally managed data management system. Specific data included the following: patient demographics; initial clinical status and cranial CT scan; and 1-year outcome, including the Glasgow Outcome Scale score on a five-point scale (18) and cognitive and physical impairment as assessed by the investigating team at each participating center via a telephone interview or via an in-person visit. A central study monitor verified all data for accuracy, consistency, and completeness.

MR Imaging Acquisition

MR imaging was performed after enrollment and as soon as MR imaging was clinically feasible, which was a mean of 23.2 days ± 1.7 (range, 7–57 days) after TBI and a mean of 13.1 days ± 1.2 (range, 5–47 days) after cardiac arrest. Vital signs were continuously monitored during imaging. Sedation, if any, was maintained. MR imaging was performed in eight centers using nine imaging units from three manufacturers (Siemens [Erlangen, Germany], GE Healthcare [Milwaukee, Wis], and Philips Healthcare [Eindhoven, the Netherlands]) and included units with both 1.5- and 3.0-T magnetic field strength. The imaging protocol has been described in previous publications (16,17). The DT imaging acquisition parameters were optimized for each MR unit, with minimal specifications of a pixel size of at most 3 × 3 × 3 mm, a B value of 1000 mT/m, and at least 12 gradient directions. The clinical team did not have access to the DT imaging results, while the investigators processing the DT imaging acquisitions (V.P. and D.G.) had no access to the clinical information and outcome of the patients. No adverse events related to MR imaging were reported.

MR Imaging Analysis

The pre- and postprocessing of the DT imaging data are described in Appendix E1 (online). This process uses nonlinear registration of $\lambda_{\parallel}$ and $\lambda_{\perp}$ maps into a standard space, as implemented in software (FLIRT/FNIRT procedures; FSL Software Technologies, New Delhi, India). The averaged $\lambda_{\parallel}$ and $\lambda_{\perp}$ values were then extracted in 19 predefined white matter regions of interest (ROIs) (Fig 1), which were selected from the white matter atlas (20). To account for intercenter and intersequence variability, these values were normalized to values of healthy control subjects by scaling each value of a patient to the mean of the corresponding parameter calculated from the healthy control subjects who underwent imaging by using the same acquisition parameters in the same center, as previously described (16,17). We tested the effects of three factors (acquisition/center, ROIs, groups) on the mean of the regional fractional anisotropy calculated in the patients and control subjects by using a three-way analysis of variance. The results showed that, before normalization, the three factors were significant ($P < .05$), and after normalization, only the group effect significantly explained the data variability. We did not adjust for the center-specific standard deviation. The intrasite coefficient of variation (ratio of the standard deviation and the mean) ranged from 2% (within the splenium of the corpus callosum) to 10% (within the body of the corpus callosum) with homogeneous variance across centers (Bartlett test). For explorative analyses, the 19 ROIs were gathered into five groups: lower brainstem region, cerebral peduncles region, corpus callosum region, right hemisphere, and left hemisphere (Fig 1). The statistical analyses of raw MR data were performed by a computer scientist (V.P., with 10 years of experience) and a mathematician (H.B., with 30 years of experience). Image analysis and quality control of MR images were performed by two neuroradiologists (D.G., with 15 years of experience, and E.T., with 10 years of experience). Data consistency and data integrity were checked by an

Figure 1

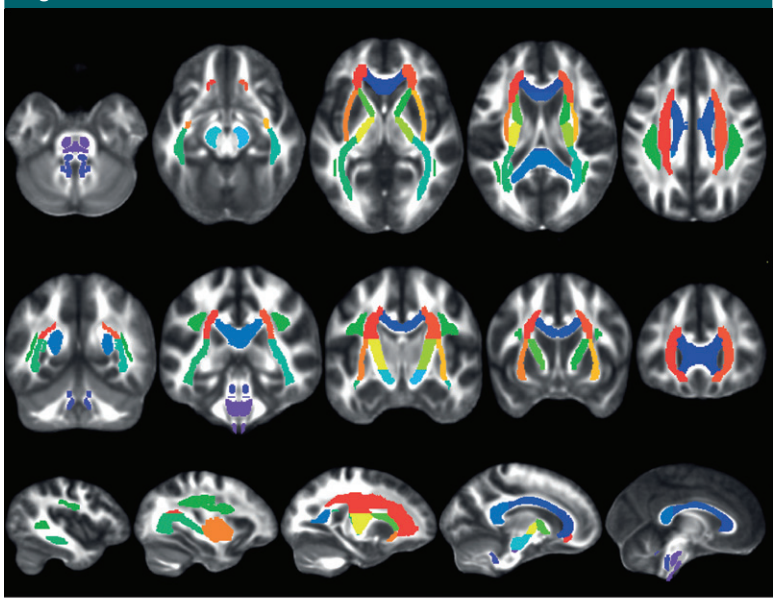

Main region	Abbreviation	Subregion
Lower brainstem	antBS	Anterior brainstem (pons, medulla oblongata)
	postBS	Posterior brainstem (pons, medulla oblongata)
Cerebral peduncles	CP_R	Right cerebral peduncle
	CP_L	Left cerebral peduncle
Corpus Callosum	gCC	Genu of the corpus callosum
	bCC	Body of the corpus callosum
	sCC	Splenium of the corpus callosum
Cerebral hemispheres	ALIC_R	Anterior arm of the internal capsule (right)
	ALIC_L	Anterior arm of the internal capsule (left)
	PLIC_R	Posterior arm of the internal capsule (right)
	PLIC_L	Posterior arm of the internal capsule (left)
	SS_R	Sagittal stratum (right)
	SS_L	Sagittal stratum (left)
	SLF_R	Superior longitudinal fasciculus (right)
	SLF_L	Superior longitudinal fasciculus (left)
	EC_R	External capsule (right)
	EC_L	External capsule (left)
	CR_R	Corona radiata (right)
	CR_L	Corona radiata (left)

Figure 1: Automatically segmented white matter ROIs for measurement of DT imaging parameters. The background images are the FMRIB58–fractional anisotropy standard space images provided in FSL. The ROIs defined by Mori et al (20) are color coded and superimposed on these background fractional anisotropy images. For explorative analyses, the color-coded ROIs in the anterior and posterior brainstem were collapsed into a single lower brainstem region; the ROIs in the cerebral peduncles were collapsed into a single cerebral peduncles region; the ROIs in the genu, splenium, and body of the corpus callosum were collapsed into a single corpus callosum region; and the ROIs in the paired anterior and posterior limbs of the internal capsule, sagittal stratum, superior longitudinal fasciculus, external capsule, and corona radiata were collapsed into right hemisphere and left hemisphere regions.

anesthesiologist (L.P., with 20 years of experience).

Statistical Analysis

Data were analyzed by using statistical software (StatView 5.0, SAS Institute, Cary, NC; and SPSS 18, SPSS, Chicago, Ill). Values are expressed as means and standard errors of the mean unless otherwise stated. Differences in demographic and clinical variables were tested by using the Student t test and the χ^2 test, as appropriate. DT imaging variables had normal distribution (according to the Kolmogorov-Smirnov test); therefore, we used parametric tests. We used the method of general linear modeling (analysis of variance with Bonferroni post hoc) for within- and between-group comparison of DT imaging variables in healthy control subjects, TBI patients, and cardiac arrest patients. Multivariate analyses were performed to evaluate the results after adjustment for age and sex. The interaction between variables was also assessed. We calculated Pearson correlation coefficients between the DT imaging parameters in each left-sided ROI and the corresponding right-sided ROI. P values were corrected for multiple testing by multiplication of the P values by the number of tested hypotheses; for example, P values were multiplied by 19 when we compared DT imaging values among the groups in the 19 ROIs (Bonferroni method). Throughout the article, we present the corrected P values. A difference with a corrected value of $P < .05$ was considered significant.

Results

The $\lambda_{\parallel}$ and $\lambda_{\perp}$ values in various brain regions of patients and healthy control subjects are illustrated in Figures 2–5.

$\lambda_{\parallel}$ and $\lambda_{\perp}$ in Patients versus Healthy Control Subjects

The $\lambda_{\parallel}$ and $\lambda_{\perp}$ in the anterior brainstem and $\lambda_{\perp}$ in the posterior brainstem were higher in cardiac arrest patients than in control subjects (all $P < .01$). The $\lambda_{\parallel}$ was lower in the posterior brainstem, and $\lambda_{\perp}$ was higher in the posterior brainstem and in the anterior brainstem

Figure 2

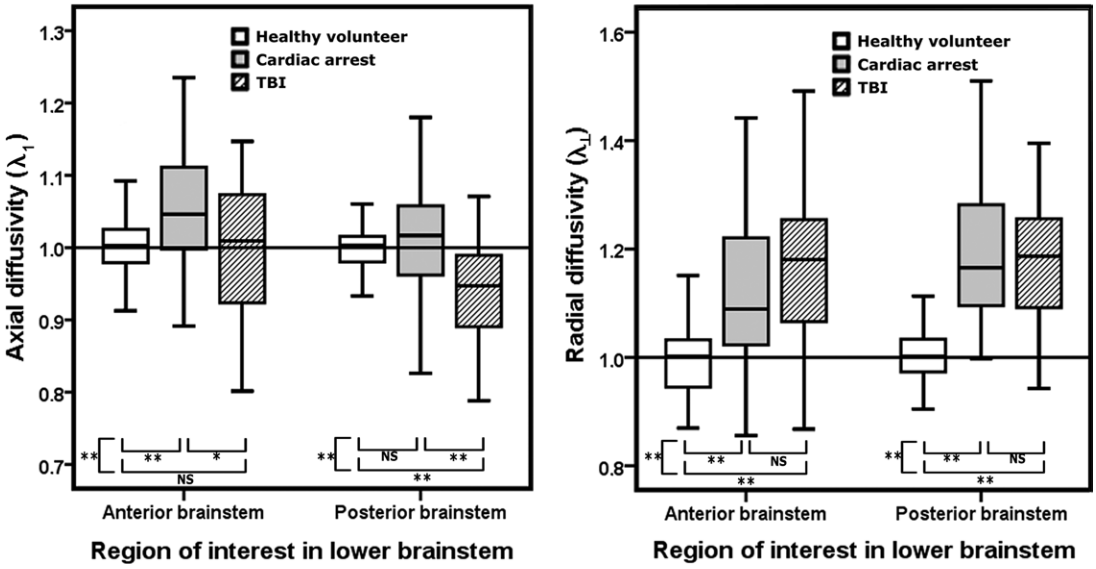

Figure 2: Normalized values of λ_1 and $\lambda_\perp$ in the lower brainstem region of patients and healthy control subjects. Box plots show the median (middle horizontal line in each box), interquartile range (25th [bottom of box] to 75th [top of box] quartiles), and the minimum (bottom of whisker) and maximum (top of whisker) values. Asterisks = *P* values for within- and between-group comparisons. When the combined ROIs were compared, *P* values with significant differences were as follows: For λ_1, TBI versus cardiac arrest patients, $P < .01$; for λ_1 and $\lambda_\perp$, TBI versus healthy control subjects and cardiac arrest patients versus healthy control subjects, $P < .01$. There were no significant interactions between the anterior and posterior brainstem. * = $P < .05$, ** = $P < .01$, NS = not significant.

Figure 3

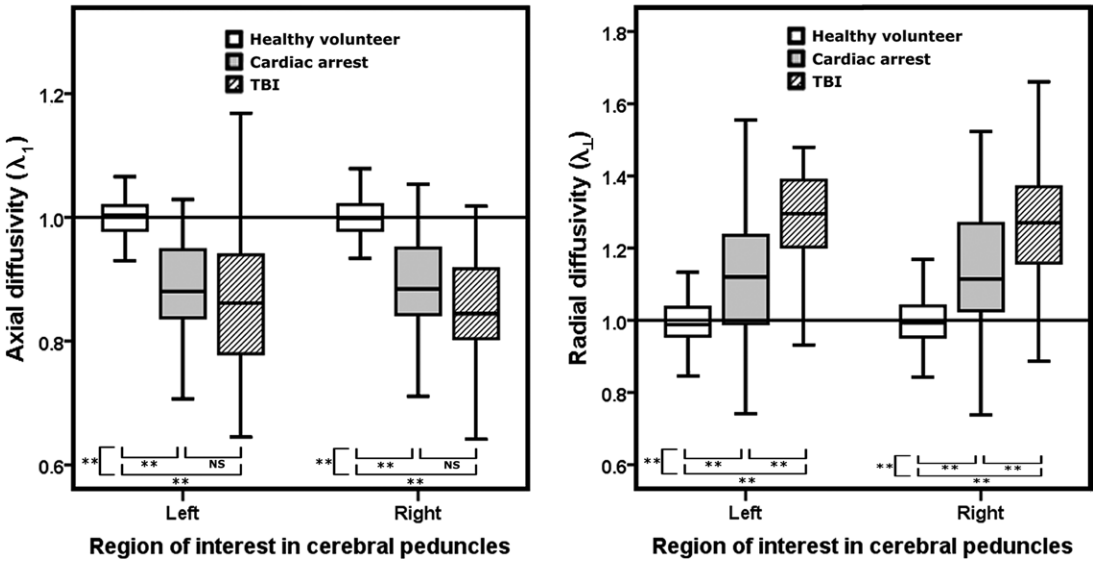

Figure 3: Normalized values of λ_1 and $\lambda_\perp$ in the cerebral peduncles region of patients and healthy control subjects. Box plots show the median (middle horizontal line in each box), interquartile range (25th [bottom of box] to 75th [top of box] quartiles), and the minimum (bottom of whisker) and maximum (top of whisker) values. Asterisks = *P* values for within- and between-group comparisons. When the combined ROIs were compared, *P* values with significant differences were as follows: For $\lambda_\perp$, TBI versus cardiac arrest patients, $P < .01$; for λ_1 and $\lambda_\perp$, TBI patients versus healthy control subjects and cardiac arrest patients versus healthy control subjects, $P < .01$. There were no significant interactions between the left and the right cerebral peduncles. ** = $P < .01$, NS = not significant.

Figure 4

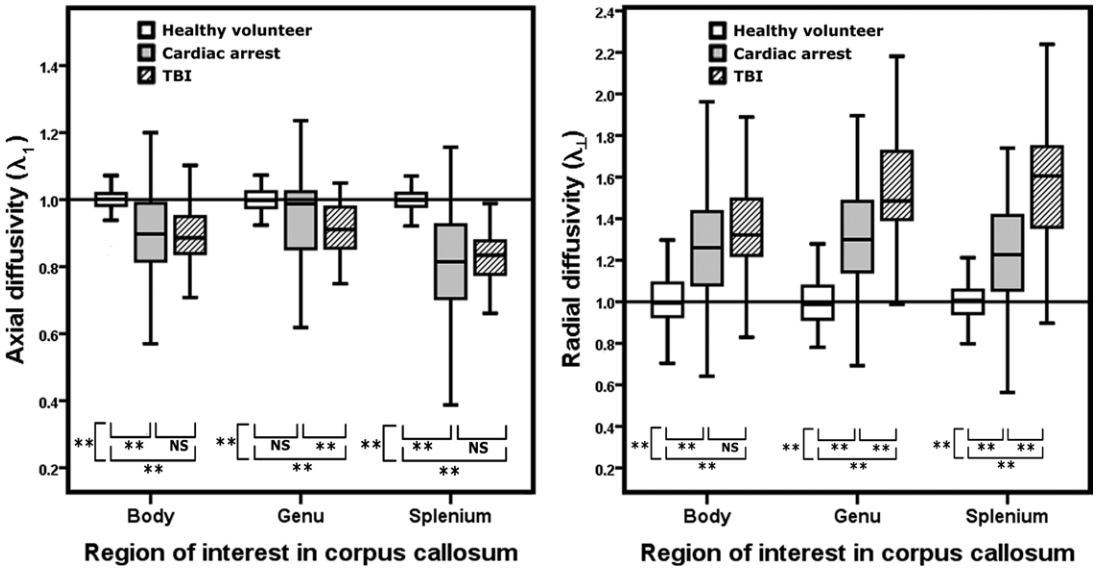

Figure 4: Normalized values of λ_1 and $\lambda_\perp$ in the corpus callosum region of patients after TBI, of patients after cardiac arrest, and of healthy control subjects. Box plots show the median (middle horizontal line in each box), interquartile range (25th [bottom of box] to 75th [top of box] quartiles), and the minimum (bottom of whisker) and maximum (top of whisker) values. Asterisks = *P* values for within- and between-group comparisons. When the combined ROIs were compared, *P* values with significant differences were as follows: For $\lambda_\perp$, TBI versus cardiac arrest patients, $P < .01$; for λ_1 and $\lambda_\perp$, TBI patient versus healthy control subjects and cardiac arrest patients versus healthy control subjects, $P < .01$. For interaction between the splenium, body, and genu for λ_1, $P < .05$, and for $\lambda_\perp$, $P < .01$. ** = $P < .01$, NS = not significant.

in TBI patients compared with control subjects (all $P < .01$) (Fig 2). The λ_1 was lower ($P < .05$) and $\lambda_\perp$ was higher ($P < .05$) in TBI patients and cardiac arrest patients than in control subjects in the left and right cerebral peduncles, body, genu, and splenium of the corpus callosum (except for λ_1 in the genu) (Figs 3, 4). Thus, in central white matter, λ_1 differed from that in control subjects in six of seven TBI ROIs and five of seven cardiac arrest ROIs (all $P < .01$). The $\lambda_\perp$ differed from that in control subjects in all ROIs in both patient groups ($P < .01$) (Figs 2–4). For the various ROIs in the cerebral hemispheres, Figure 5 shows the comparison of λ_1 and $\lambda_\perp$ in patients versus in control subjects. Thus, in hemispheres, λ_1 was decreased compared with that in control subjects in three of 12 TBI ROIs ($P < .05$) and nine of 12 cardiac arrest ROIs ($P < .01$). The $\lambda_\perp$ was increased in all TBI ROIs ($P < .01$) and in seven of 12 cardiac arrest ROIs ($P < .05$). Cerebral hemisphere λ_1 was lower in cardiac arrest than in TBI in six of 12 ROIs ($P < .01$), while $\lambda_\perp$ was higher in TBI than in cardiac arrest in eight of 12 ROIs ($P < .01$).

λ_1 and $\lambda_\perp$ in Cardiac Arrest versus TBI Patients

The major findings for the difference in λ_1 and $\lambda_\perp$ between TBI and cardiac arrest patients are reported in Figures 2–5. Table 2 presents the type and distribution of abnormalities in central regions (anterior and posterior brainstem, left and right cerebral peduncles, genu, body, and splenium of the corpus callosum) and in cerebral hemispheric regions (left and right sagittal strata, superior longitudinal fasciculus, anterior and posterior limb of internal capsule, external capsule, and corona radiata). In both central regions and cerebral hemispheres, $\lambda_\perp$ was higher ($P < .05$) in TBI patients than in cardiac arrest patients. In cerebral hemispheres, λ_1 was lower ($P < .05$) in cardiac arrest patients than in TBI patients.

The differences presented in Figures 2–4 remained significant after adjustment for age and sex.

λ_1 and $\lambda_\perp$ in the Left versus the Right Cerebral Hemisphere

Figure 5 shows a symmetrical pattern of DT imaging changes in the ROIs in the corresponding right and left hemispheres in patients with cardiac arrest and in control subjects. Indeed, there was a significant intercorrelation between DT imaging values of the ROIs in the corresponding right and left hemispheres in cardiac arrest patients (ranging from $r = 0.81$ in the external capsule to $r = 0.99$ in the corona radiata for λ_1 and from $r = 0.73$ in the external capsule to $r = 0.99$ in the corona radiata for $\lambda_\perp$; $P < .001$) and in control subjects (ranging from $r = 0.73$ in the sagittal stratum to $r = 0.84$ in the anterior limb of the internal capsule

Figure 5

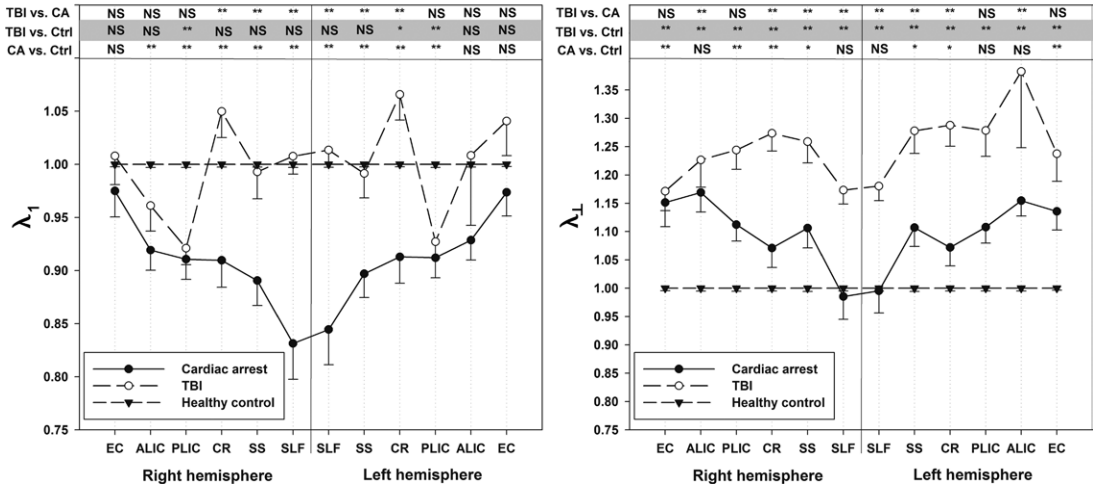

Figure 5: Normalized values of λ_1 and $\lambda_\perp$ in the cerebral hemispheres of patients and healthy control subjects. The right hemisphere is at left, and the left hemisphere is at right. Asterisks = *P* values for within- and between-group comparisons. Symbols in each line = mean for each member of the group indicated; error bars = standard errors of the mean. For interaction between the ROIs in the right hemisphere for both λ_1 and $\lambda_\perp$, $P < .01$; for interaction between the ROIs in the left hemisphere for λ_1, $P < .01$. Notice the symmetrical pattern of involvement for λ_1 in TBI and cardiac arrest patients and for $\lambda_\perp$ in cardiac arrest patients, while the pattern of involvement for $\lambda_\perp$ in TBI patients is asymmetric. * = $P < .05$, ** = $P < .01$, *ALIC* = anterior limb of internal capsule, *CA* = cardiac arrest, *CR* = corona radiata, *Ctrl* = healthy control subject, *EC* = external capsule, *NS* = not significant, *PLIC* = posterior limb of internal capsule, *SLF* = superior longitudinal fasciculus, *SS* = sagittal stratum.

Table 2

Types and Distribution of Abnormalities in TBI and Cardiac Arrest Patients

Diffusivity and Pathologic Finding	Central Regions*	Cerebral Hemispheres†
λ_1		
Cardiac arrest	−8.9 ± 12.1	−9.1 ± 14.7
TBI	−9.4 ± 7.0	−0.1 ± 9.9
$\lambda_\perp$		
Cardiac arrest	20.2 ± 23.1	9.7 ± 20.7
TBI	37.5 ± 20.4	24.9 ± 16.8

Note.—Data are the mean percentage increases or decreases of the patients' values as compared with those of the healthy control subjects ± standard deviations. The denominator of each percentage is, per definition, 1.0, which is the mean relative λ_1 or $\lambda_\perp$ in the discussed region in healthy control subjects. *P* values were less than .01 for comparison of λ_1 or $\lambda_\perp$ between cardiac arrest and TBI patients for central regions and cerebral hemispheres, but the *P* value of .53 was not significant for comparison of λ_1 between cardiac arrest and TBI patients for the central regions.

* The central regions represent the anterior and posterior brainstem, the left and right cerebral peduncles, the genu, the body, and the splenium of the corpus callosum.

† The cerebral hemispheres represent the left and right sagittal strata, the superior longitudinal fasciculus, the anterior and posterior limb of the internal capsule, the external capsule, and the corona radiata.

for λ_1 and from $r = 0.75$ in the external capsule to $r = 0.93$ in the corona radiata for $\lambda_\perp$; $P < .001$; values close to one represent symmetry between DT imaging values in the ROIs in the corresponding left and right hemispheres). In TBI patients, this symmetrical pattern of DT imaging changes was not seen for most ROIs (Table 3).

Discussion

This article shows that DT imaging can help distinguish the different pathophysiologic mechanisms that underly similar states of impaired consciousness following TBI and cardiac arrest.

Our main findings are a marked decrease in λ_1 in cardiac arrest patients and a marked increase in $\lambda_\perp$ in TBI patients. These findings are consistent with reported pathophysiologic concepts, a fact that supports the validity of DT imaging to help distinguish axonal and myelin damage in vivo in groups of patients. Thus, in cardiac arrest, the marked decrease in λ_1 is consistent with primary axonal damage (6,10–13) related to energy depletion from anoxic ischemia. Primary axonal damage induces changes in the fluid microenvironment of the central nervous system, to which in turn myelin is susceptible (21–24). The moderate $\lambda_\perp$ increases in our cardiac arrest patients are consistent with such secondary myelin damage (25). Conversely, the marked $\lambda_\perp$ increase in many areas of TBI patients suggests myelin damage, edema, and/or macrophage infiltration as the primary injury. The mechanical forces exerted on the brain in TBI probably cause more myelin damage than axonal damage. The smaller λ_1 decrease in TBI patients is consistent with axonal damage, caused either by direct trauma (axonotmesis) or by indirect ischemic damage secondary to extracranial traumatic injuries. In a later phase, brain swelling and increased intracranial pressure may further contribute to the axonal damage. In cardiac arrest, there is a gradient of injury severity from the cerebral hemispheres toward the medulla oblongata, with relative sparing of the central brain structures (26). The vascular anatomy in the cerebral hemispheres,

Table 3

Intercorrelations between DT Imaging Values in Corresponding ROIs in the Left and Right Hemispheres

Group and Parameter	EC	ALIC	PLIC	CR	SS	SLF
Control subjects*						
λ_1	0.76	0.84	0.80	0.81	0.73	0.81
$\lambda_\perp$	0.75	0.79	0.86	0.93	0.91	0.89
Cardiac arrest patients*						
λ_1	0.81	0.93	0.97	0.99	0.97	0.98
$\lambda_\perp$	0.73	0.80	0.93	0.99	0.98	0.98
TBI patients						
λ_1	0.48†	0.11	0.51‡	0.42†	0.24	0.33
$\lambda_\perp$	0.31	0	0.60*	0.15	0.21	0

Note.—The data in the table are the correlation coefficients between DT imaging values of the right and left hemispheres in the various ROIs; for example, 0.76 is the correlation coefficient between λ_1 values in the right and left external capsules in healthy control subjects. Values close to one indicate side-to-side symmetry in DT imaging values. ALIC = anterior limb of internal capsule, CR = corona radiata, EC = external capsule, PLIC = posterior limb of internal capsule, SLF = superior longitudinal fasciculus, SS = sagittal stratum.

* $P < .001$.

† $P < .05$.

‡ $P < .01$.

characterized by widespread linear arterioles with few anastomoses, increases the vulnerability of the hemispheric white matter to hypoxic-ischemic injury (27–29). Conversely, in TBI patients, $\lambda_\perp$ was highly abnormal in both the central brain structures and the cerebral hemispheres. This finding is consistent with the distribution of diffuse axonal injury observed in the classic monkey model of axial trauma caused by rotational and acceleration-deceleration shearing forces (30). The $\lambda_\perp$ increase and, to a lesser extent, the λ_1 decrease were asymmetric, being more pronounced in the left cerebral hemisphere of our TBI patients. This predominance of left-sided abnormalities in TBI patients with poor clinical outcomes was expected, as left-sided lesions are more frequently symptomatic. The asymmetry was attributable to a left predominance of $\lambda_\perp$ abnormalities and, to a lesser extent, λ_1 abnormalities, suggesting greater asymmetry of edema and/or myelin damage than of axonal damage. This finding supports the hypothesis that edema and myelin damage are chiefly related to the mechanical trauma, which is an asymmetric assault, whereas axonal damage may be a combined effect of symmetric systemic processes and asymmetric local processes.

Our finding of greater $\lambda_\perp$ as compared with λ_1 alterations in TBI patients is consistent with DT imaging findings in the key experimental mouse model of brain injury by Mac Donald et al (10). The researchers in all previous descriptive DT imaging studies in humans at the early subacute phase of TBI evaluated a later or longer time window than we did in our study (31–36), included patients with milder brain injury (33,36–38), and/or did not specify separate diffusivity parameters in various ROIs (33,35,36,38,39). As intuitively expected, $\lambda_\perp$ values and therefore myelin damage played a larger role than λ_1 in a recent DT imaging–based and clinically based prognostic model in severe TBI (17). To our knowledge, no previous descriptive DT imaging studies in human cardiac arrest patients have been published.

To our knowledge, investigators in only one previous study (40) have compared the use of DT imaging in cardiac arrest patients versus TBI patients. Our finding of greater severity of central brain structure injury in TBI patients versus cardiac arrest patients is consistent with the findings in the comparative study at a later postinjury phase of Newcombe et al (40). Although an overall λ_1 decrease was our main finding in cardiac arrest patients, λ_1 in the lower brainstem and cerebral peduncles regions showed larger decreases in TBI than in cardiac arrest. Similarly, in a study of 30 patients with severe TBI evaluated 8 weeks after trauma, λ_1 was decreased and $\lambda_\perp$ was increased in the deep brain regions and brainstem (31,41). Whereas we found large differences in the cerebral hemispheres between cardiac arrest and TBI, Newcombe et al (40) found broadly similar DT imaging abnormalities in TBI and ischemic-hypoxic brain injury. This discrepancy is ascribable to differences in patient populations and MR imaging timing, as well as to the relatively small number of patients studied by Newcombe et al.

Our study had several limitations. As was inevitable with a multicenter design, the DT imaging data were acquired with different MR imaging machines. We corrected for this source of variability by normalizing the patient values to values in healthy control subjects who underwent imaging with the same parameters on the same machine. Because of the epidemiology of TBI and cardiac arrest, our TBI patients were younger and cardiac arrest patients had higher mortality rates. Differences in treatment-limitation decisions between the two patient groups cannot be ruled out. We followed up the patients for 1 year. Although improvements are unlikely to occur beyond this period, some degree of conformation bias cannot be ruled out. In both cardiac arrest and TBI, neurologic injury and recovery is a dynamic process. Therefore, our findings are only valid within the studied time (ie, the early subacute phase [42]). In TBI, the spatial distribution varies across patients as a result of variations in the direction of the impact on the head. That highly significant results were found in our study despite this inevitable source of heterogenity supports the general applicability of our findings.

Our results should be tested in future research evaluating the robustness

and validity of $\lambda_{\parallel}$ and $\lambda_{\perp}$, preferably comparing the DT imaging results with postmortem pathologic findings.

Although the neurologic presentation is similar in patients with persistent consciousness impairments after TBI and cardiac arrest, DT imaging findings suggest substantial differences in white matter injury between these two causes. Our findings indicate differences at both the topographic and the cellular levels. The results in cardiac arrest patients are consistent with a primary axonal injury responsible for secondary myelin damage. In TBI in contrast, the chiefly mechanical primary mechanism results in myelin damage, which is followed by secondary ischemic injury. The consistency of our findings with current pathophysiologic concepts supports the validity of DT imaging for in vivo testing of pathophysiologic hypotheses in humans. DT imaging is a promising in vivo tool for separating myelin from axonal damage, a step that may prove important in the early prediction and understanding of patient outcomes.

Acknowledgment: We acknowledge Ritse Mann for editing Figures 2, 3, and 4.

Disclosures of Conflicts of Interest: **A.W.v.d.E.** No relevant conflicts of interest to disclose. **O.K.** No relevant conflicts of interest to disclose. **V.P.** No relevant conflicts of interest to disclose. **J.D.** No relevant conflicts of interest to disclose. **P.S.** No relevant conflicts of interest to disclose. **P.E.V.** Financial activities related to the present article: none to disclose. Financial activities not related to the present article: author as head of steering committee and institution received payment for consultancy from Ever Neuropharma. Other relationships: none to disclose. **C.E.L.** Financial activities related to the present article: none to disclose. Financial activities not related to the present article: received payment for board membership from Bayer, received grants or has grants pending from Janssen Cilag, and received payment for lectures including service on speakers bureaus from MSD and Thermo-Fischer Brahms. Other relationships: none to disclose. **R.D.S.** Financial activities related to the present article: none to disclose. Financial activities not related to the present article: employed by Johns Hopkins University and received grants or has grants pending from DARPA. Other relationships: none to disclose. **N.M.d.C.** No relevant conflicts of interest to disclose. **C.D.** No relevant conflicts of interest to disclose. **E.T.** No relevant conflicts of interest to disclose. **R.G.** No relevant conflicts of interest to disclose. **D.D.** No relevant conflicts of interest to disclose. **S.L.** No relevant conflicts of interest to disclose. **H.B.** No relevant conflicts of interest to disclose. **A.V.** No relevant conflicts of interest to disclose. **D.G.** No relevant conflicts of interest to disclose. **L.P.** Financial activities related to the present article: institution received a grant from PHRC AOM 2005. Financial activities not related to the present article: received payment for consultancy from Actelion. Other relationships: none to disclose.

References

1. Elovic E, Baerga E, Cuccurullo S. Mechanism and recovery of head injury. In: Cuccurullo S, ed. Physical medicine and rehabilitation board review. New York, NY: Demos Medical Publishing, 2004; http://www.ncbi.nlm.nih.gov/books/NBK27256/.
2. Ringelstein EB, Stogbauer F. Border zone infarcts. In: Bogousslavsky J, Caplan L, eds. Stroke syndromes. 2nd ed. Cambridge, England: Cambridge University Press, 2001; 564–582.
3. Lövblad KO. Hypoxic-ischemic Lesions. In: Von Kummer R, Back T, eds. Magnetic resonance imaging in ischemic stroke. Berlin, Germany: Springer, 2005; 239–250.
4. Okamura T, Ishibashi N, Kumar TS, et al. Hypothermic circulatory arrest increases permeability of the blood brain barrier in watershed areas. Ann Thorac Surg 2010;90(6): 2001–2008.
5. Kumar R, Woo MA, Macey PM, Fonarow GC, Hamilton MA, Harper RM. Brain axonal and myelin evaluation in heart failure. J Neurol Sci 2011;307(1-2):106–113.
6. Song SK, Sun SW, Ramsbottom MJ, Chang C, Russell J, Cross AH. Dysmyelination revealed through MRI as increased radial (but unchanged axial) diffusion of water. Neuroimage 2002;17(3):1429–1436.
7. Alexander AL, Lee JE, Lazar M, Field AS. Diffusion tensor imaging of the brain. Neurotherapeutics 2007;4(3):316–329.
8. Xie M, Tobin JE, Budde MD, et al. Rostrocaudal analysis of corpus callosum demyelination and axon damage across disease stages refines diffusion tensor imaging correlations with pathological features. J Neuropathol Exp Neurol 2010;69(7):704–716.
9. Beaulieu C. The basis of anisotropic water diffusion in the nervous system: a technical review. NMR Biomed 2002;15(7-8): 435–455.
10. Mac Donald CL, Dikranian K, Bayly P, Holtzman D, Brody D. Diffusion tensor imaging reliably detects experimental traumatic axonal injury and indicates approximate time of injury. J Neurosci 2007; 27(44):11869–11876.
11. Mac Donald CL, Dikranian K, Song SK, Bayly PV, Holtzman DM, Brody DL. Detection of traumatic axonal injury with diffusion tensor imaging in a mouse model of traumatic brain injury. Exp Neurol 2007;205(1): 116–131.
12. Song SK, Sun SW, Ju WK, Lin SJ, Cross AH, Neufeld AH. Diffusion tensor imaging detects and differentiates axon and myelin degeneration in mouse optic nerve after retinal ischemia. Neuroimage 2003;20(3): 1714–1722.
13. Sun SW, Liang HF, Trinkaus K, Cross AH, Armstrong RC, Song SK. Noninvasive detection of cuprizone induced axonal damage and demyelination in the mouse corpus callosum. Magn Reson Med 2006;55(2):302–308.
14. Takahashi M, Ono J, Harada K, Maeda M, Hackney DB. Diffusional anisotropy in cranial nerves with maturation: quantitative evaluation with diffusion MR imaging in rats. Radiology 2000;216(3):881–885.
15. Song SK, Yoshino J, Le TQ, et al. Demyelination increases radial diffusivity in corpus callosum of mouse brain. Neuroimage 2005; 26(1):132–140.
16. Luyt CE, Galanaud D, Perlbarg V, et al. Diffusion tensor imaging to predict long-term outcome after cardiac arrest: a bicentric pilot study. Anesthesiology 2012;117(6):1311–1321.
17. Galanaud D, Perlbarg V, Gupta R, et al. Assessment of white matter injury and outcome in severe brain trauma: a prospective multicenter cohort. Anesthesiology 2012;117(6):1300–1310.
18. Jennett B, Bond M. Assessment of outcome after severe brain damage. Lancet 1975;1(7905):480–484.
19. Marshall LF, Marshall SB, Klauber MR, et al. The diagnosis of head injury requires a classification based on computed axial tomography. J Neurotrauma 1992;9(suppl 1): S287–S292.
20. Mori S, Oishi K, Jiang H, et al. Stereotaxic white matter atlas based on diffusion tensor imaging in an ICBM template. Neuroimage 2008;40:570–582.
21. Lennon VA, Whittingham S, Carnegie PR, McPherson TA, Mackay IR. Detection of antibodies to the basic protein of human myelin by radioimmunoassay and immunofluorescence. J Immunol 1971;107(1):56–62.
22. Sharma HS, Zimmer C, Westman J, Cervós-Navarro J. Acute systemic heat stress increases glial fibrillary acidic protein immunoreactivity in brain: experimental observa-

tions in conscious normotensive young rats. Neuroscience 1992;48(4):889–901.

23. Sharma HS, Kretzschmar R, Cervós-Navarro J, Ermisch A, Rühle HJ, Dey PK. Age-related pathophysiology of the blood-brain barrier in heat stress. Prog Brain Res 1992;91:189–196.

24. Sharma HS, Olsson Y, Cervós-Navarro J. p-Chlorophenylalanine, a serotonin synthesis inhibitor, reduces the response of glial fibrillary acidic protein induced by trauma to the spinal cord: an immunohistochemical investigation in the rat. Acta Neuropathol (Berl) 1993;86(5):422–427.

25. Sharma HS, Miclescu A, Wiklund L. Cardiac arrest-induced regional blood-brain barrier breakdown, edema formation and brain pathology: a light and electron microscopic study on a new model for neurodegeneration and neuroprotection in porcine brain. J Neural Transm 2011;118(1):87–114.

26. Miller JR, Myers RE. Neuropathology of systemic circulatory arrest in adult monkeys. Neurology 1972;22(9):888–904.

27. Ginsberg MD, Myers RE. The topography of impaired microvascular perfusion in the primate brain following total circulatory arrest. Neurology 1972;22(10):998–1011.

28. Ginsberg MD, Hedley-Whyte ET, Richardson EP Jr. Hypoxic-ischemic leukoencephalopathy in man. Arch Neurol 1976;33(1):5–14.

29. Busl KM, Greer DM. Hypoxic-ischemic brain injury: pathophysiology, neuropathology and mechanisms. NeuroRehabilitation 2010;26(1):5–13.

30. Ommaya AK, Gennarelli TA. Cerebral concussion and traumatic unconsciousness: correlation of experimental and clinical observations of blunt head injuries. Brain 1974;97(4):633–654.

31. Sidaros A, Engberg AW, Sidaros K, et al. Diffusion tensor imaging during recovery from severe traumatic brain injury and relation to clinical outcome: a longitudinal study. Brain 2008;131(Pt 2):559–572.

32. Le TH, Mukherjee P, Henry RG, Berman JI, Ware M, Manley GT. Diffusion tensor imaging with three-dimensional fiber tractography of traumatic axonal shearing injury: an imaging correlate for the posterior callosal "disconnection" syndrome—case report. Neurosurgery 2005;56(1):189.

33. Arfanakis K, Haughton VM, Carew JD, Rogers BP, Dempsey RJ, Meyerand ME. Diffusion tensor MR imaging in diffuse axonal injury. AJNR Am J Neuroradiol 2002;23(5):794–802.

34. Newcombe VF, Williams GB, Nortje J, et al. Analysis of acute traumatic axonal injury using diffusion tensor imaging. Br J Neurosurg 2007;21(4):340–348.

35. Nakayama N, Okumura A, Shinoda J, et al. Evidence for white matter disruption in traumatic brain injury without macroscopic lesions. J Neurol Neurosurg Psychiatry 2006;77(7):850–855.

36. Ptak T, Sheridan RL, Rhea JT, et al. Cerebral fractional anisotropy score in trauma patients: a new indicator of white matter injury after trauma. AJR Am J Roentgenol 2003;181(5):1401–1407.

37. Kumar R, Saksena S, Husain M, et al. Serial changes in diffusion tensor imaging metrics of corpus callosum in moderate traumatic brain injury patients and their correlation with neuropsychometric tests: a 2-year follow-up study. J Head Trauma Rehabil 2010;25(1):31–42.

38. Inglese M, Makani S, Johnson G, et al. Diffuse axonal injury in mild traumatic brain injury: a diffusion tensor imaging study. J Neurosurg 2005;103(2):298–303.

39. Huisman TA, Schwamm LH, Schaefer PW, et al. Diffusion tensor imaging as potential biomarker of white matter injury in diffuse axonal injury. AJNR Am J Neuroradiol 2004;25(3):370–376.

40. Newcombe VF, Williams GB, Scoffings D, et al. Aetiological differences in neuroanatomy of the vegetative state: insights from diffusion tensor imaging and functional implications. J Neurol Neurosurg Psychiatry 2010;81(5):552–561.

41. Parvizi J, Damasio AR. Neuroanatomical correlates of brainstem coma. Brain 2003;126(pt 7):1524–1536.

42. Weiss N, Galanaud D, Carpentier A, Naccache L, Puybasset L. Clinical review: prognostic value of magnetic resonance imaging in acute brain injury and coma. Crit Care 2007;11(5):230.